NASA Technical Memorandum 103937

Issues and Approach to Develop Validated Analysis Tools for Hypersonic Flows: One Perspective

George S. Deiwert

November 1992

National Aeronautics and Space Administration

NASA Technical Memorandum 103937

Issues and Approach to Develop Validated Analysis Tools for Hypersonic Flows: One Perspective

George S. Deiwert, Ames Research Center, Moffett Field, California

November 1992

National Aeronautics and
Space Administration

Ames Research Center
Moffett Field, California 94035-1000

1. Summary

Critical issues concerning the modeling of low-density hypervelocity flows where thermochemical nonequilibrium effects are pronounced are discussed. Emphasis is on the development of validated analysis tools. A description of the activity in the Ames Research Center's Aerothermodynamics Branch is also given. Inherent in the process is a strong synergism between ground test and real-gas computational fluid dynamics (CFD). Approaches to develop and/or enhance phenomenological models and incorporate them into computational flow-field simulation codes are discussed. These models have been partially validated with experimental data for flows where the gas temperature is raised (compressive flows). Expanding flows, where temperatures drop, however, exhibit somewhat different behavior. Experimental data for these expanding flow conditions is sparse, and reliance must be made on intuition and guidance from computational chemistry to model transport processes under these conditions. Ground-based experimental studies used to provide necessary data for model development and validation are described. Included are the performance characteristics of high-enthalpy flow facilities, such as shock tubes and ballistic ranges.

2. Introduction

The development of validated analysis tools for hypersonic flows involves a process in which real-gas CFD development and application and experimental testing are performed hand in hand, synergistically, until the validation is complete. Hypersonic flows inherently involve real-gas phenomena. The validation of CFD tools requires considerations associated with perfect-gas CFD validation plus consideration of additional complexities associated with real-gas phenomena. These complexities include thermal and chemical time scales, multiple gas species, internal energy flow variables and properties, and coupled fluid/chemical processes.

That it is not possible to fully simulate real-gas hypersonic flight conditions in ground-test facilities is axiomatic. Ground-test experiments must be carefully selected to validate basic principles and concepts in CFD codes. It is necessary to use CFD in the design of experiments, in the definition of the test environment, in the development, application, and interpretation of diagnostics, and in the analysis of the test results as a whole. The test data then form a basis for validating the process and the CFD tools. The CFD codes can be used to extrapolate to flight conditions. And, finally, flight experiments are required to confirm the process as a whole.

These concepts will be developed, in part, in this paper, and illustrative examples will be presented. First, the problem will be characterized in terms of aspects of real-gas behavior and features associated with high-enthalpy, hypervelocity ground-test facilities. Next, real-gas phenomena will be discussed as they relate to both aerodynamic performance and aerothermo heating of hypersonic vehicles. Finally, the process of developing validated analysis tools will be described as represented by selected examples of ongoing research in the Aerothermodynamics Branch of Ames Research Center.

3. Characteristics of Real Gas

The character of a real gas is described by the internal degrees of freedom and state of its constituent molecules, nitrogen and oxygen. The internal energy states of the molecules, rotational, vibrational, and electronic, are excited, and, in the limit, the molecular bonds are exceeded and the gas dissociated into atomic, and possibly ionic, constituents. The process of energy transfer causing excitation, dissociation, and recombination is a rate process controlled by particle collisions. Binary, two-body collisions are sufficient to cause internal excitation, dissociation, and ionization, while three-body collisions are required to recombine the particles into molecular constituents. If the rates of energy transfer are fast with respect to the local fluid-dynamic time scale, the gas is in, or nearly in, equilibrium. If the energy transfer rates are very slow, the gas can be described as frozen. In all other instances, wherein any of the energy exchange rates are comparable to the local fluid time scale, the gas will be thermally or chemically reacting and out of equilibrium.

Each of these definitive states of a real gas (equilibrium, chemically frozen, or reacting) can be possible in a gas undergoing compression and heating, such as the gas flowing through a strong shock ahead of a bluff body, or in an expanding and cooling gas, such as a gas flowing away from a stagnation region of a bluff body or a gas expanding into a base region. In the first case, the gas will be thermally excited and will dissociate and ionize; in the second case, the atomic constituents will recombine and the internal energy states will relax to lower energy levels.

A real gas implies the existence of any, or all, of the above states. This includes the possibility that a real gas can look identical to a perfect gas or a chemically frozen gas. In a real-gas flow the model scale is a primary test variable. The possibility exists to generate a spectrum of real-gas test conditions at a single geometrically similar test point. These flows can vary from frozen to equilibrium flow.

For chemically frozen flow there is little value to real-gas experimentation on the nose region; if the flow is frozen at the stagnation point it will remain frozen as it expands throughout the blunt nose and over the afterbody, where it may equilibrate. Nose-region information for such a flow will be identical to perfect-gas wind-tunnel results and can be predicted reliably within the limits of our knowledge of thermodynamic and transport properties. Afterbody data, however, may be of greater interest, particularly data describing flow over secondary surfaces that may induce further chemical activity.

Similarly, for chemical equilibrium flow, real-gas experiments are not required. In this case, the extrapolation from a perfect gas to a real gas is straightforward, involving appropriate thermodynamic and transport properties for the reacting gas species.

Between the two limits, in the region of reacting gas flows, is the greatest uncertainty and the greatest need for test data. The facilities required for CFD validation of high-enthalpy flows must be capable of generating a reacting gas flow over configurations of interest and must have sufficient diagnostic ability to provide the information necessary to describe the character and behavior of the flow.

4. Real-Gas Test Facilities

In principle, there are two ways to create relative motion between the test article and the air: accelerate the air (as in a shock tunnel) or accelerate the model (as in a ballistic range). Both techniques are now being used, and both are needed to give insight into real-gas phenomena. The two concepts have also been combined to create even higher relative speeds, as in the Ames Hypersonic Free-Flight Aerodynamic Facility (HFFAF) where a large shock tunnel is utilized to provide counterflow to an aeroballistic range.

Ballistic ranges represent a unique capability for real-gas testing of configurations. They present the only experimental technique by which real-gas viscous-interaction effects can be observed. Shock tunnels, because of the nature of their expansion process, do not generate sufficiently high test Mach numbers where viscous-interaction phenomena would be important.

To date, most data presented from ballistic range facilities have been integrated aerodynamic data on simple geometric configurations. Early efforts by Welch (ref. 1) demonstrated a significant real-gas effect on the center-of-pressure and moment data. More recent data by Strawa (refs. 2–4) continue these studies. Validation requires not only overall aerodynamic data but also data on distributions of local flow-field quantities within the shock and boundary layer of the tested configuration. Aerodynamic coefficient data are determined through the motions of the model down the length of the tube. Drag and static moment can be determined in about half a period of motion, lift coefficient requires 1.5 to 2 cycles, and damping coefficients require even more. Recent advances (ref. 5) in automated data-taking and data-reduction techniques have resulted in significant improvements in the accuracy of aerodynamics coefficients and the efficiency with which they are determined.

In-stream flow-field data can be determined from in-flight shadowgraphs and laser holographic interferometry (refs. 6 and 7). These data provide quantitative information on shock shape and position, turbulence onset, and in-stream density distribution and supplement integrated aerodynamic coefficient data for CFD validation purposes. An advantage of ballistic range testing is that the free stream is accurately characterized and can precisely simulate the flight environment.

Shock tunnels currently offer the only means of producing both the total enthalpy and pressure levels representative of flight beyond Mach 10. Shock tubes and shock tunnels do not precisely simulate flight environment, however, and flow-accelerated test facilities require the free stream to be defined. In supersonic test facilities this has been accomplished through the use of isentropic flow-expansion models. Real-gas accelerations are not isentropic. Realistic CFD models of the expansion process must be used in conjunction with critical (but not exhaustive) instrumentation to fully define the free stream. The fluid-dynamic and thermodynamic states of chemically reacting air (including N, O, N_2, O_2, and NO) in the HFFAF 16-in. shock tunnel were characterized accounting for viscous effects in an axisymmetric nozzle. These results are compared in figure 1 with conventional quasi-one-dimensional real-gas simulations to identify the magnitude of viscous and geometric effects in a real-gas environment. Complete calibration of a real-gas nozzle-expansion process can be achieved only through this collaboration between insightful, limited measurements and increasingly accurate CFD models of the expansion process. Complex real-gas flows require the use of full test section calibrations with the key measurements being the free-stream density and static temperature. CFD validation must include facility simulation; we must not pretend to simulate flight with flow-accelerated ground tests.

5. Real-Gas Effects

5.1 Aerodynamic Performance

Real-gas effects are important in the determination of vehicle aerodynamic performance, e.g., aerodynamics coefficients, control surface behavior, onset of transition, and relaminarization. One example that illustrates this is the aerodynamic performance of the Space Shuttle during entry.

The Space Shuttle orbiter flight-test program has required the aerodynamicist to take a new approach in determining flight characteristics. The initial series of flights of the orbiter were heavily instrumented for the purpose of obtaining accurate aerodynamic data. The flight data derived from the entry Mach range provided for comparisons between flight- and wind-tunnel-derived predicted data in the areas of both aerodynamic performance and longitudinal trim. Romere and Whitnah (ref. 8) examined these data and showed that, in the continuum flight regime (altitudes below about 85 km), lift and drag were smaller during the orbiter flights than predicted by ground tests in perfect-gas wind tunnels. The center of pressure (CP) is displaced forward by as much as 0.7% of the overall fuselage length compared with predictions based on perfect-gas observations. This result, which is attributed to real-gas effects, is quite large considering that the full deflection of the control surfaces was expected to produce a CP shift of, at most, about 1% of the overall length. A plot showing the comparison of CP location determined from flight data with preflight predictions is shown in figure 2. Griffith and Maus (ref. 9) show that the observed discrepancy is due, at least in part, to the high-temperature real-gas effects.

Rakich et al. (ref. 10) explain this phenomenon by performing a computational study of real-gas flows over simple wedges and cones and the flow over the orbiter's forebody. The nonequilibrium flow over a pointed cone at zero incidence is described in a qualitative manner as shown in figure 3, which illustrates the variation in bow shock shape and the distribution of a typical species, i.e., atomic oxygen, over the conical forebody. Even though the body is conical, the flow has a scale that depends on the time constant for pertinent species reactions. Near the apex of the cone there is a region where time is insufficient for reactions to occur. Here the flow is conical, and the species concentrations are nearly frozen at their free-stream values. As the fluid moves downstream of the apex, the species begin to thermalize and the flow is out of equilibrium. Far downstream, all of the reactions have equilibrated, and even those reactions induced locally by the bow shock equilibrate in a short distance relative to the larger shock standoff distance. A quantitative description is shown in figure 4, where the computed variation of bow shock angle is shown for a 30-degree half-angle wedge at conditions corresponding to an altitude of 65.5 km and a flight speed of 6.7 km/s. These conditions are typical of the high-laminar-heating portion of the orbiter's entry trajectory. And finally, in figure 5 is shown the computed shock shapes for the orbiter's forebody for both a perfect gas and a reacting gas. These computations correspond to a flight speed of 6.7 km/s, an altitude of 65.5 km, and an angle of incidence of 30 degrees.

Recently, Park and Yoon (ref. 11) performed a computational study of real-gas effects on airfoil aerodynamic characteristics. The results of this study showed that the aerodynamic lift and drag coefficients are consistently reduced by thermochemical real-gas phenomena, and that, for air, the behavior can be represented by a value of γ less than the perfect gas value of 1.4. The computed center of pressure was observed to shift forward due to the thermochemical phenomena, but the extent of the shift is also sensitive to geometry and angle of attack and cannot be represented by a fixed value for γ. The calculated results are illustrated in figure 6 for an airfoil of chord length 10 m, at an altitude of 74 km, a speed of 7 km/s, and an angle of incidence of 40 degrees. These results are in qualitative agreement with the data obtained during the entry flights of the Space Shuttle orbiter. Included are results for a reacting-air gas and results for perfect gas at constant γ values of 1.4 and 1.2. The constant-γ-of-1.2 solution agrees well with real-gas predictions for lift and drag but fails to adequately represent the CP shift between a real-gas solution and γ-of-1.4 solution.

5.2 Aerothermal Heating

Real-gas thermochemical nonequilibrium processes are also important in the determination of aerodynamic heating, both convective (including wall catalytic effects) and radiative. To illustrate this we consider the hypervelocity flow over a bluff body typical of an atmospheric-entry vehicle or an aerospace transfer vehicle (ASTV).

The qualitative aspects of a hypersonic flow field over a bluff body are discussed in two parts, forebody and afterbody, with attention to which particular physical effects must be included in an analysis. This discussion will indicate what type of numerical modeling will be adequate in each region of the flow.

5.2.1 Forebody flow field– A bluff forebody flow field, illustrated schematically in figure 7, is dominated by the presence of the strong bow shock wave and the consequent heating and chemical reaction of the gas. At high-altitude hypersonic flight conditions, the thermal excitation and chemical reaction of the gas occur slowly enough

that a significant portion of the flow field is in a state of thermochemical nonequilibrium. A second important effect is the presence of the thick boundary layer along the forebody's surface. In this region there are large thermal and chemical species gradients due to the interaction of the gas with the wall. Also, at high altitudes the shock wave and the boundary layer may become so thick that they merge; in this case the entire shock layer is dominated by viscous effects.

A gas is in thermal nonequilibrium if, for a given density and internal energy, it is in a thermodynamic state where the internal energy modes cannot be characterized by a unique temperature; a gas is in chemical nonequilibrium if its chemical state does not satisfy chemical equilibrium conditions. As was asserted above, a portion of the forebody's flow field is in thermochemical nonequilibrium. This can be seen by observing the trajectory of a control volume of air that enters the shock layer. The translational modes of this volume of gas are heated strongly as it passes through the bow shock wave. The translational modes transfer their energy to the other internal energy modes of the molecules through intermolecular collisions.

Also, chemical reactions of the gas species occur, such as dissociation and ionization. These processes require a series of intermolecular collisions for equilibrium to be reached. Thus as the volume element of gas is convected through the shock layer, these energy exchanges and chemical reactions occur at a finite rate until, at some point on the streamline, equilibrium is achieved. Therefore, there will be significant thermochemical nonequilibrium near the bow shock wave, and equilibrium will be approached a large distance along the fluid element's streamline.

The rate at which equilibration is realized is dependent on the free-stream density and speed, or altitude and Mach number. A parameter that quantifies the degree of chemical nonequilibrium for a particular condition is the Damkohler number, the ratio of the fluid time scale to the chemical time scale; a similar parameter may be derived for the relaxation of energy modes.

The second important effect in the forebody region is the interaction of the wall with the thermally excited and reacted gas in the boundary layer. At the high altitudes the Reynolds number is relatively small (typically on the order of 10^4 based on free-stream conditions and nose radius). Thus the boundary layer will be thick, and viscous effects will dominate much of the flow field. Also, as the boundary layer is influenced by the cool wall, chemical reactions can be slowed or halted in the vicinity of the wall. The wall can also interact chemically with the flow field due to catalytic effects that promote the recombination of reacted species at the wall. Thus, the inclusion of viscous effects for hypersonic bluff forebody flow-field analyses is mandatory. At high altitudes, the usual assumption of perfect thermal accommodation and no-slip at the wall breaks down. Therefore, for some conditions, temperature and velocity slip effects must also be included.

Another effect related to the low-density regime in which ASTVs would operate is the thickening of the bow shock wave to encompass a large volume of the flow field. The bow shock wave is several mean-free-paths thick, and at high altitudes, this implies that the bow shock thickness is an appreciable fraction of the shock standoff distance and can merge with the thick boundary layer. For these thick shock waves, relaxation of internal modes occurs within the shock wave; this effect must be included in any analysis where rarefaction occurs. Also, it has been shown that the Navier-Stokes equations underpredict the shock thickness and misrepresent the separation between the density and temperature profiles within a shock wave (ref. 12). Thus, for some regimes, the predicted shock thickness using Navier-Stokes solvers is suspect.

5.2.2 Afterbody flow field– The flow about an afterbody, illustrated in figure 8, is dominated by two phenomena: the presence of rapid expansion as the highly compressed gas flows around the shoulder of the vehicle, and the related initiation of separation of the gas near the vehicle's corner. These two effects require specific modeling approaches and capabilities.

The expansion, which is dominated by inviscid effects, has the effect of rapidly lowering the translational temperature, density, and pressure of the gas. However, the chemical state of the gas and the temperatures that characterize the energy in the internal modes will tend to remain constant, or frozen. This results in a flow where the vibrational and electronic temperatures of the gas are far higher than the translational temperature and where the gas is more dissociated and excited than predicted by equilibrium conditions. As the gas flows downstream, recombination occurs slowly and the vibrational temperature rises still higher, a result of a portion of the chemical energy of recombination being put into the vibrational modes of the gas. This can cause the gas to radiate significantly in the afterbody region.

Another result observed in the inviscid, expanded region is the presence of species gradients across the wake. This is caused by some portion of the gas having passed through a relatively weak oblique shock wave, where reactions are weak, and another part of the gas having passed through the strong forebody shock, where reactions are strong. Thus the gas near the center of the wake tends to be more dissociated than that in its

extremities; consequently γ, the ratio of specific heats, varies across the wake.

Another observation associated with the wake structure is the presence of a wake shock. As the flow expands around the shoulder of the vehicle, some of it is directed toward the centerline of the body. However, this supersonic flow must change direction, and a reflecting shock and an oblique shock wave is formed. The gas becomes compressed in this region, yet the vibrational and electronic temperatures remain high due to freezing, and the gas may radiate significantly.

The location of the separation on the back face of the bluff body is affected by: the state of the boundary layer on the shoulder, the Reynolds number, whether the flow is turbulent or laminar, the ratio of specific heats, and the body geometry. For many cases of interest, particularly at high altitude, the flow can remain attached over a significant portion of the vehicle's afterbody. The location of separation influences the dimension of the recirculation zone and the strength of the shear layer that forms between the recirculating gas and the external, rapidly expanding, supersonic flow. The recirculation zone entrains gas, formerly in the forebody boundary layer, that is relatively cool but highly dissociated. This recirculation zone will be unsteady, the magnitude of which depending on how the shear layer behaves and on the feedback between the body motion and the state of the gas in the separated region.

The modeling of the free shear layer must account for large gradients of velocity, temperature, density, and species concentration across it, and for the possibility that the flow may be turbulent and unsteady. The numerical treatment of the problem is particularly difficult because of these effects and also because of the uncertain location of this layer.

The afterbody flow field is characterized by the presence of thermochemical nonequilibrium, large gradients in thermodynamic quantities and chemical state, and a large separated region. The combination of these factors stretches CFD beyond its current capabilities.

6. Illustrative Examples

6.1 Aerodynamic Trim

To acquire data necessary to validate and/or calibrate real-gas code capability to predict aerodynamic performance, the aeroballistic range is proposed. Ballistic range data will include visual flow-field data indicating shock shape and location relative to the body (i.e., by way of shadowgraphs) and density distribution (i.e., by holographic interferograms) as well as quantitative information in the form of aerodynamic coefficients, including lift, drag, and pitching moment. The use of a combination of CFD with experiment has proved most effective in the interpretation of free-flight data. For example, in a recent study on trim angle for the NASA Aeroassist Flight Experiment (AFE) vehicle (ref. 5), there was insufficient free-flight data for determining high-order terms for series-expansion representation of aerodynamic coefficients. In order to extract information from the experimental data, the curvature of the function describing the moment coefficient was required. This curvature was developed using CFD. For the analysis of data from the Ames HFFAF aeroballistic range, the higher-order terms in the aerodynamic coefficient expansion were determined from CFD simulations; only the lower-order terms were found by using a six-degree-of-freedom, weighted, least-squares procedure. The resulting experimental aerodynamic coefficients and trim angles agree with those computed by CFD. The effective specific-heat ratio for the HFFAF was determined by matching the bow shock shape and stand-off distance with CFD perfect-gas, constant effective γ, flow-field simulations at the HFFAF test conditions. Results of these comparisons are shown in figure 9, in which the CFD simulation bow shock is identified by a coalescence of isobars.

AFE model moment coefficient data from the HFFAF are compared (see fig. 10) with data from two NASA Langley hypersonic cold-flow facilities, the 31-in. Mach-10 tunnel and the CF_4 tunnel. Each of the three facilities can be identified by an effective γ: 1.2 for HFFAF, 1.34 for the Mach-10 tunnel, and 1.11 for the CF_4 tunnel. The measured trim angles are 14.7, 17, and 12 degrees, respectively.

By minimizing the uncertainty in trim angle, design tolerances can be tightened and vehicle configurations can be optimized for specific mission requirements. By using a combination of CFD analysis and ground-based experiments, the real-gas effects can be simulated, analysis tools validated, and flight conditions estimated with some confidence. In many cases the aeroballistic range can be used to simulate actual flight conditions, and reasonable estimates of aerodynamic trim angle and pitching moment for flight can be determined directly. The agreement shown herein between experimental and computed results for the blunt AFE configuration at the ground test conditions indicates that, at these test conditions, the moment coefficients and trim angles can be computed using efficient ideal-gas solvers with an appropriate choice for γ; the appropriate value of this parameter can be determined by comparing shock shapes. This is not necessarily the case, however, for slender or high-lift vehicles. In cases where actual flight conditions cannot be replicated in ground test facilities, real-gas solvers must be used to

determine if constant effective γ approximations are appropriate. As mentioned previously, the variations in γ at flight conditions can have a sizable influence on aerodynamic moment coefficient and trim angle.

6.2 Aerothermodynamic Heating

6.2.1 Compressive flows– To study the nonequilibrium processes in compressing flow typical of the stagnation region of a bluff forebody, we are looking in some detail at a gas relaxing after being heated by an incident shock wave. By acquiring normal shock in a spectrally clean facility, we are able to quantify the thermochemical state of the gas as a function of time or position. By this means, we can study such processes as vibration-dissociation coupling, vibration-translation exchange, vibration-rotation coupling, etc. (refs. 13–15).

The dominant real-gas phenomenon is the relaxation process occurring in the flow around hypersonic vehicles. Considerable effort has been expended in recent years to model and numerically compute this behavior (e.g., refs. 16–19). The accuracy of such calculations needs further improvement, and there are still many physical parameters that are unknown for high-temperature real gases. Three types of experimental data are needed in this model-development process: (1) data which will enhance our phenomenological understanding of the relaxation process, (2) data on rates for the relevant reactions, and (3) data on bulk properties, such as spectral radiation emitted by the gas, for a given set of aerodynamic conditions. We are collecting such data by simulating the required aerothermochemical conditions in an electric-arc-driven shock tube (refs. 20 and 21). NASA Ames' electric-arc-driven shock tube facility is powered by a 0.6-MJ, 40-kV capacitor bank and is capable of producing shock velocities in the range of 2–50 km/sec. The radiation diagnostic system available at the facility consists of (1) a linear intensified 700-element diode array and (2) a 2-D intensified CCD array with 576 × 384 active elements, both gateable within a time range of 30 ns–2.5 ms and both with a 2000–8000-A spectral response. A photomultiplier tube (PMT) is used to record the total radiation from the test gas as well as from the driver gas as they pass through the test section. The signal from the PMT is used to estimate the test time and to trigger the diode array system at a given moment during the test. A Nd:YAG-laser-based, double-exposure, single-plate interferometer is also available at the facility. A schematic of the experimental test setup is shown in figure 11.

A one-dimensional real-gas flow code for thermochemical nonequilibrium (refs. 22 and 23) is used to predict the thermochemical state of the shock-heated gas behind the incident shock. This code uses a multiple-temperature description to model the nonequilibrium behavior of the internal state of the gas and to describe the rate processes. From the predicted thermochemical state of the gas, synthetic emission spectra can be generated. For this we use the computer code NEQAIR (refs. 24 and 25). Several modeling steps are involved in this process. First are the chemical rate expressions themselves, in which there is always some uncertainty in the Arrhenius rate constants, second is the multiple-temperature model used to describe both the internal energy states of the gas and the reaction rates, and third is the quasi-steady-state model and peripheral approximations used to generate the synthetic spectra in the NEQAIR code. By maintaining a coordinated effort between the modeling activity and the experimental effort it is possible both to improve and refine the phenomenological models as well as to validate them. These models will then, in turn, be used in multidimensional flow codes to predict and analyze real-gas behavior in more complex flow environments.

To date, two sets of experiments have been conducted: (1) measurements at a shock velocity of 6.20 km/sec in 1 torr nitrogen (ref. 26) and (2) measurements at a shock velocity of 10.2 km/sec in 0.1 torr air (ref. 27). In both the sets, using the linear diode array, the equilibrium and nonequilibrium spectra covering the 3050–5500-A range were recorded.

Measurements in nitrogen (6.2 km/sec, 1.0 torr): For the nitrogen case, the equilibrium temperature of the test gas based on $N_2(2^+)$ band system was found to be 6500 K. The rotational temperature at the point of peak radiation in the nonequilibrium region, based on the intensities at 3143.7 A and 3159.1 A, was found to be about 8800 K. The vibrational temperature, based on the first vibrational level and the ground state of the $N_2(2^+)$ band system, was found to be about 6900 K. The temperatures based on higher vibrational levels were lower.

The equilibrium temperature of the test gas, based on the $N_2^+(1^-)$ band system, was found to be 7200 K. The rotational temperature at the point of peak radiation in the nonequilibrium region was deduced to be about 8800 K, which is consistent with the value found by using the $N_2(2^+)$ band system. Comparisons of rotational temperature with prediction and with earlier data from Allen et al. (ref. 28) are shown in figure 12. The vibrational temperature, as measured based on the v(1,2)/v(1,0) levels of the $N_2^+(1^-)$ band system, was found to be about 9500 K, with the value decreasing for higher vibrational levels. The temperature based on the v(7,8) vibrational level was about 8500 K. Comparisons of vibrational temperature with prediction and with earlier data are shown in figure 13.

Measurements in air (10.2 km/sec, 0.1 torr): For shock-heated air the equilibrium temperature was estimated to be 9620 K. The equilibrium emission spectra observed are shown in figure 14. By using two different sets of points on the rotational envelope of the $N_2(2^+)$ band system, the rotational temperatures, corresponding to the point of peak radiation, were estimated to be about 4400 K and 3990 K, respectively, making a mean rotational temperature of 4195 K. Such a low value of rotational temperature was a surprise. The overshoot observed in the nitrogen tests at 6.2 km/sec was absent here. The rotational temperature seems to rise very slowly to reach the equilibrium value. The emission spectra observed at the point of peak radiation are shown in figure 15.

The vibrational temperature at the point of peak radiation was deduced using the (2,1) and (3,2) bands of $N_2^+(1^-)$ system at 3564.1 and 3548.2 A, respectively, and was found to be about 9465 K. There were no other vibrational temperature data available for these conditions. The measured vibrational temperatures based on $N_2^+(1^-)$ as well as based on $N_2(2^+)$ band systems are in line with the theoretical values as predicted by Park's model (ref. 17). Sharma (ref. 20) shows further details, analysis of the experimental data, and comparisons with theory.

6.2.2 Expanding flows– To study the nonequilibrium processes in an expanding flow as typified by the flow over the shoulder of a bluff body and into the base, or near-wake, region, we look at a gas that has been shock heated to high temperature and pressure and allowed to expand rapidly in a two-dimensional nozzle. By using optical diagnostics such as laser holographic interferometry and Raman scattering (ref. 29), we can quantify the thermochemical state of the gas during the expansion process. Nonequilibrium vibrational populations for levels up to v = 8 have been measured in an expanding flow, using the spontaneous Raman scattering technique. A nozzle insert has been installed in the driven section operating in a reflected shock mode. The density flow field was mapped by laser-based holography. The results of this initial test are shown in figure 16, where good agreement can be observed between computer-simulated and experimental fringe interferograms.

7. Concluding Remarks

In summary, it has been pointed out that real-gas effects are important in hypersonic flows both in terms of their influence on aerodynamic performance and their effect on aerothermdynamic heating. Further, it was pointed out that high-enthalpy, ground-based test facilities cannot fully simulate flight conditions and that they exhibit unique real-gas behavior themselves. Hence, the process for developing validated analysis tools is one where real-gas CFD is involved in all aspects of a real-gas ground test program. Only in this manner can sufficient confidence be gained and real-gas analysis tools be validated.

References

1. Welch, C. J.; Lawrence, W. R.; and Watt, R. M.: Real-Gas Effects on the Aerodynamics of Blunt Cones as Measured in a Hypervelocity Range. AEDC TR 79-33.
2. Strawa, A. W.; Chapman, G. T.; Canning, T. C.; and Arnold, J. O.: The Ballistic Range and Aerothermodynamic Testing. AIAA Paper 88-2015.
3. Strawa, A. W.; and Prabhu, D. K.: A Comparison of Experimental and Computational Results for 5- and 10-Degree Cones at High Mach Numbers. AIAA Paper 88-2705.
4. Strawa, A. W.; Molvik, G.; Yates, L.; and Cornelison, C.: Experimental and Computational Results for 5-Degree Blunt Cones with Shock Generators at High Velocity. AIAA Paper 89-3377.
5. Yates, L. A.; and Venkatapathy, E.: Trim Angle Measurements in Free-Flight Facilities. AIAA Paper 91-1632.
6. Strawa, A. W.; and Cavolowsky, J. A.: Development of Non-Intrusive Instrumentation for NASA-Ames' Ballistic Range and Shock Tunnel. AIAA Paper 90-0628.
7. Tam, T. C.; Brock, N. J.; Cavolowsky, J. A.; and Yates, L. A.: Holographic Interferometry at the NASA-Ames Hypervelocity Free-Flight Aerodynamic Facility. AIAA Paper 91-0568.
8. Romere, P. O.; and Whitnah, A. M.: Space Shuttle Entry Longitudinal Aerodynamic Comparisons of Flights 1–4 with Preflight Predictions. In Shuttle Performance Lessons Learned, NASA CP-2283, 1983.
9. Griffith, B. J.; and Maus, J. R.: Explanation of the Hypersonic Longitudinal Stability Problem—Lessons Learned. In Shuttle Performance Lessons Learned, NASA CP-2283, 1983.

10. Rakich, J. V.; Bailey, H. E.; and Park, C.: Computations of Nonequilibrium, Supersonic Three-Dimensional Inviscid Flow over Blunt-Nosed Bodies. AIAA J., vol. 21, no. 6, June 1983, pp. 834–841.

11. Park, C.; and Yoon, S.: A Fully Coupled Implicit Method for Thermo-Chemical Nonequilibrium Air at Sub-Orbital Flight Speeds. AIAA Paper 89-1974.

12. Fiscko, K. A.; and Chapman, D. R.: Hypersonic Shock Structure with Burnett Terms in the Viscous Stress and Heat Flux. AIAA Paper 88-2733.

13. Park, C.: Two-Temperature Interpretation of Dissociation Rate Data for N_2 and O_2. AIAA Paper 88-0458.

14. Sharma, S.; Huo, W.; and Park, C.: The Rate Parameters for Coupled Vibration-Dissociation in a Generalized SSH Approximation. AIAA Paper 88-2714.

15. Park, C.: A Review of Reaction Rates in High-Temperature Air. AIAA Paper 89-1740.

16. Candler, G. V.; and MacCormack, R. W.: The Computation of Hypersonic Ionized Flows in Chemical and Thermal Nonequilibrium. AIAA Paper 88-0511.

17. Candler G. V.; and Park C.: The Computation of Radiation from Nonequilibrium Hypersonic Flows. AIAA Paper 88-2678.

18. Gokcen, T.; and MacCormack: Nonequilibrium Effects for Hypersonic Transitional Flows Using Continuum Approach. AIAA Paper 89-0461.

19. Candler, G. V.: On the Computation of Shock Shapes in Nonequilibrium Hypersonic Flows. AIAA Paper 89-0312.

20. Sharma, S.; and Park, C.: A Survey of Simulation and Diagnostic Techniques for Hypersonic Nonequilibrium Flows. AIAA Paper 87-0406.

21. Sharma, S.; and Park, C.: Operating Characteristics of a 60-cm and a 10-cm Electric-Arc-Driven Shock Tube. AIAA Paper 88-0142.

22. Park, C.: Assessment of Two-Temperature Kinetic Model for Dissociating and Weakly Ionizing Nitrogen. J. Thermophysics and Heat Transfer, vol. 2, no. 1, Jan. 1988, pp. 8–16.

23. Park, C.: Assessment of Two-Temperature Kinetic Model for Ionizing Air. J. Thermophysics and Heat Transfer, vol. 3, no. 3, July 1989, pp. 233–244.

24. Park, C.: Nonequilibrium Air Radiation (NEQAIR) Program: User's Manual. NASA TM-86707, July 1985.

25. Whiting, E.; and Patterson, J.: Recent Advances at NASA in Calculating The Electronic Spectra of Diatomic Molecules. NASA TM-101034, Oct. 1988.

26. Sharma, S.: Nonequilibrium and Equilibrium Shock Front Radiation Measurements. AIAA Paper 90-0139.

27. Sharma, S.; Gillespie, W. D.; and Meyer, S. A.: Shock Front Radiation Measurements in Air. AIAA Paper 91-0573.

28. Allen, R. A.; Camm, J. C.; and Keck, J. C.: Radiation from Hot Nitrogen. AVCO-Everett Research Laboratory Report 102, April 1961.

29. Sharma, S.; Ruffin, S.; Meyer, S. A.; Gillespie, W. D.; and Yates, L. A.: Density Measurements in an Expanding Flow Using Holographic Interferometry. AIAA Paper 92-0809.

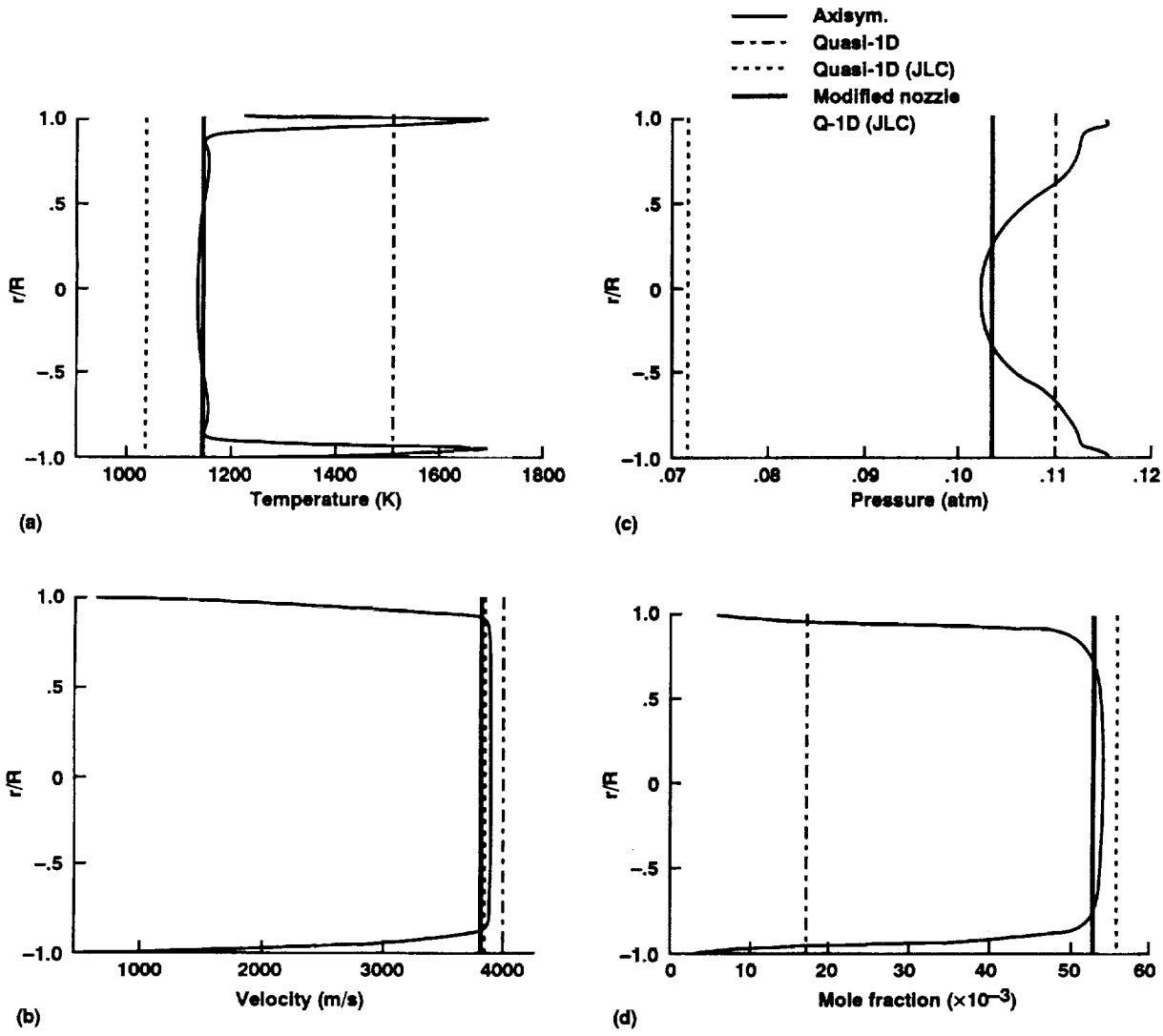

Figure 1. Ames 16-Inch Shock Tunnel nozzle exit profiles from real-gas CFD prediction. (a) Temperature, (b) axial velocity, (c) static pressure, (d) atomic oxygen mole fraction.

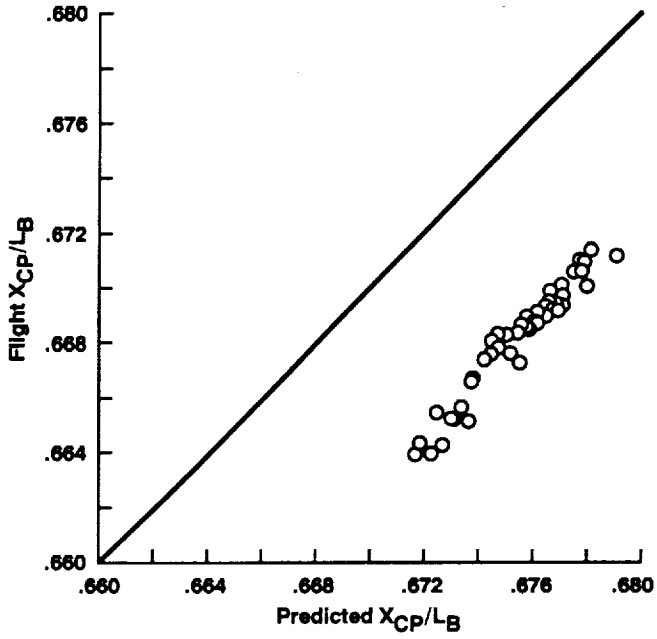

Figure 2. Hypersonic longitudinal aerodynamic center-of-pressure correlation of flight with predicted data for pullup/pushover maneuvers; STS-2, M = 21.

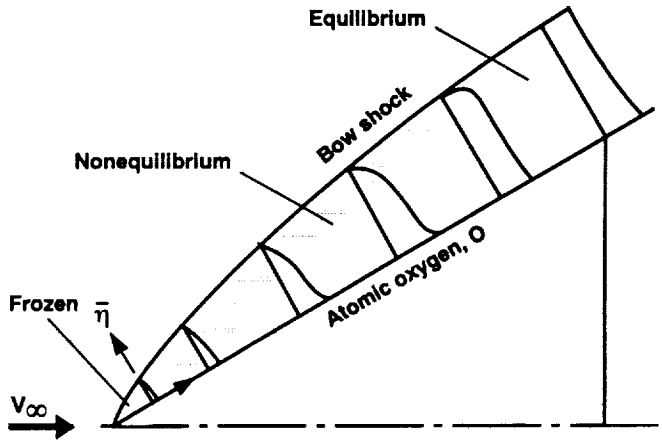

Figure 3. Schematic profiles of atomic oxygen between body and shock of a pointed cone.

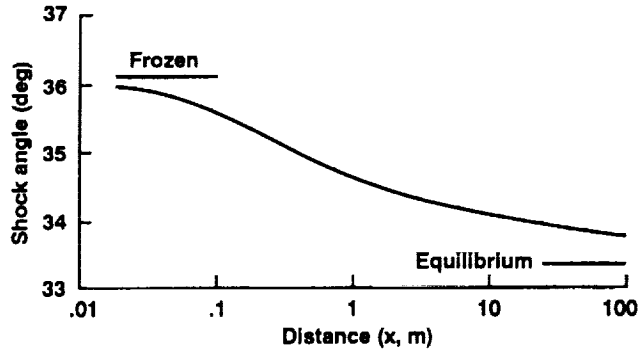

Figure 4. Shock angle for nonequilibrium flow over a 30-deg wedge.

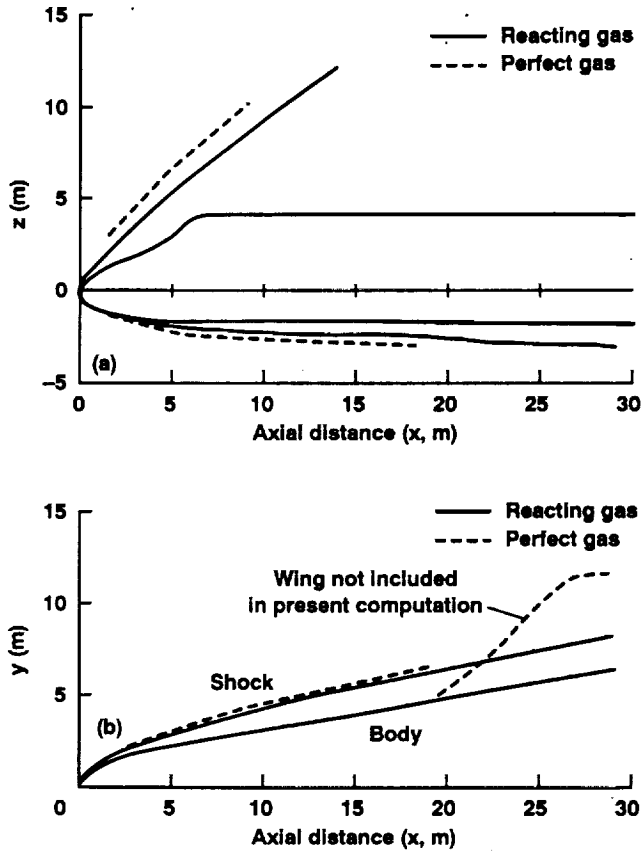

Figure 5. Shock shape for Shuttle 147 body; a = 30 deg, V = 6.7 km/s, altitude = 65.5 km. (a) Side view; (b) plan view.

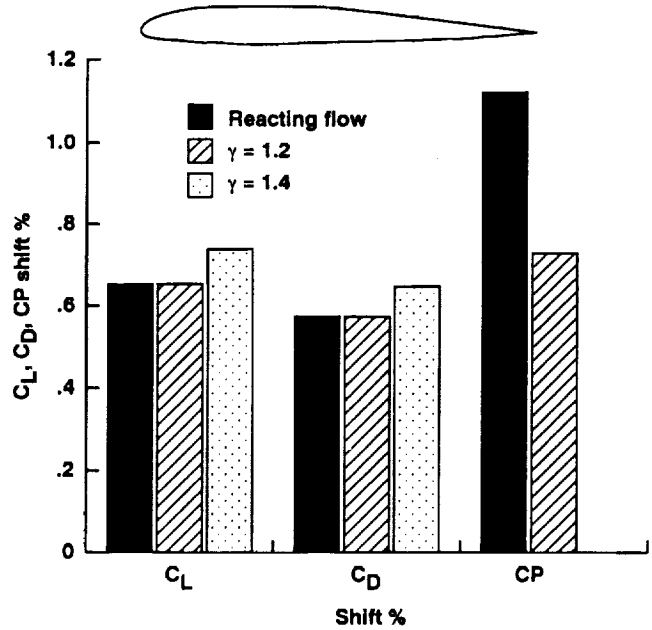

Figure 6. Lift and drag coefficients and CP shift for airfoil; chord = 10 m, altitude = 74 km, V = 7 k/s, α = 40 deg.

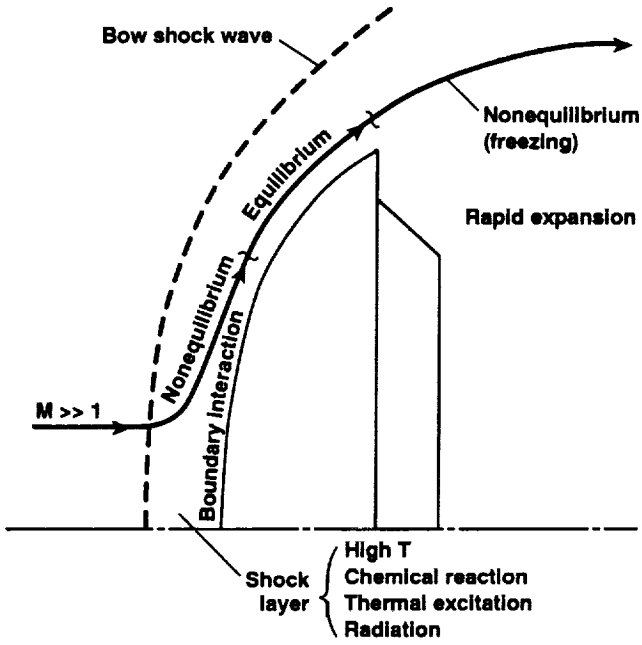

Figure 7. Schematic of hypervelocity bluff forebody flow field.

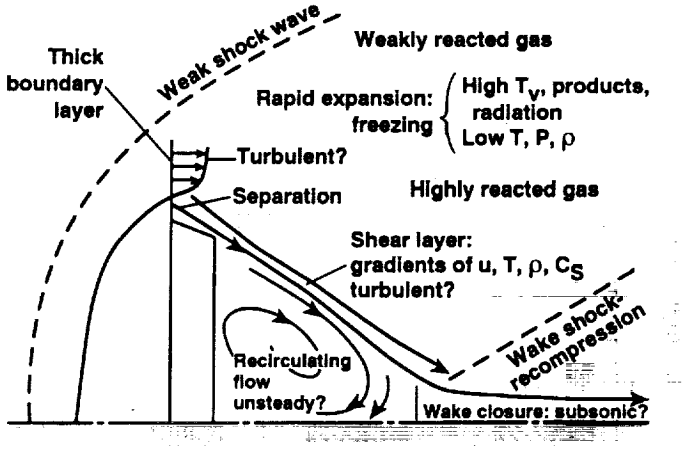

Figure 8. Schematic of hypervelocity bluff-body near-wake flow field.

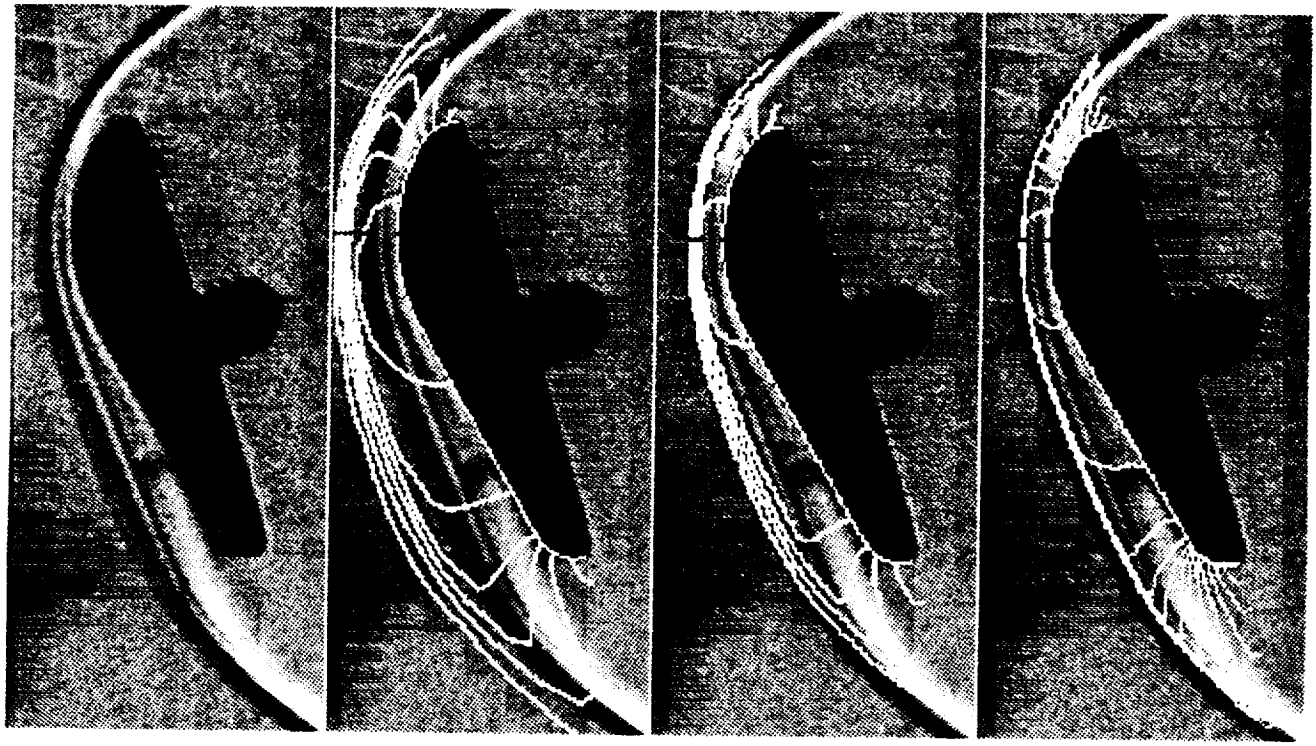

Figure 9. Experimental and computed AFE bow shock.

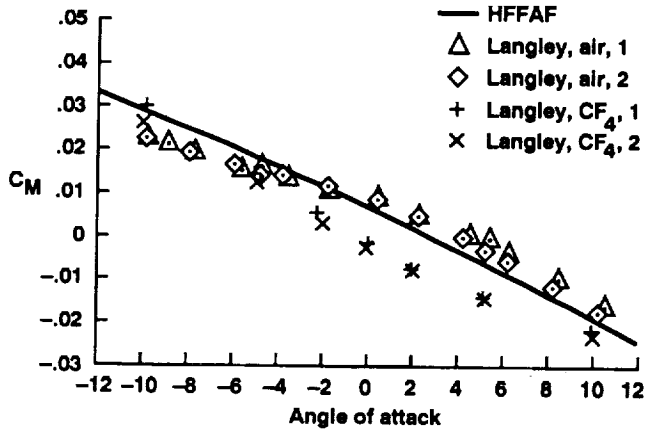

Figure 10. AFE moment coefficient comparison.

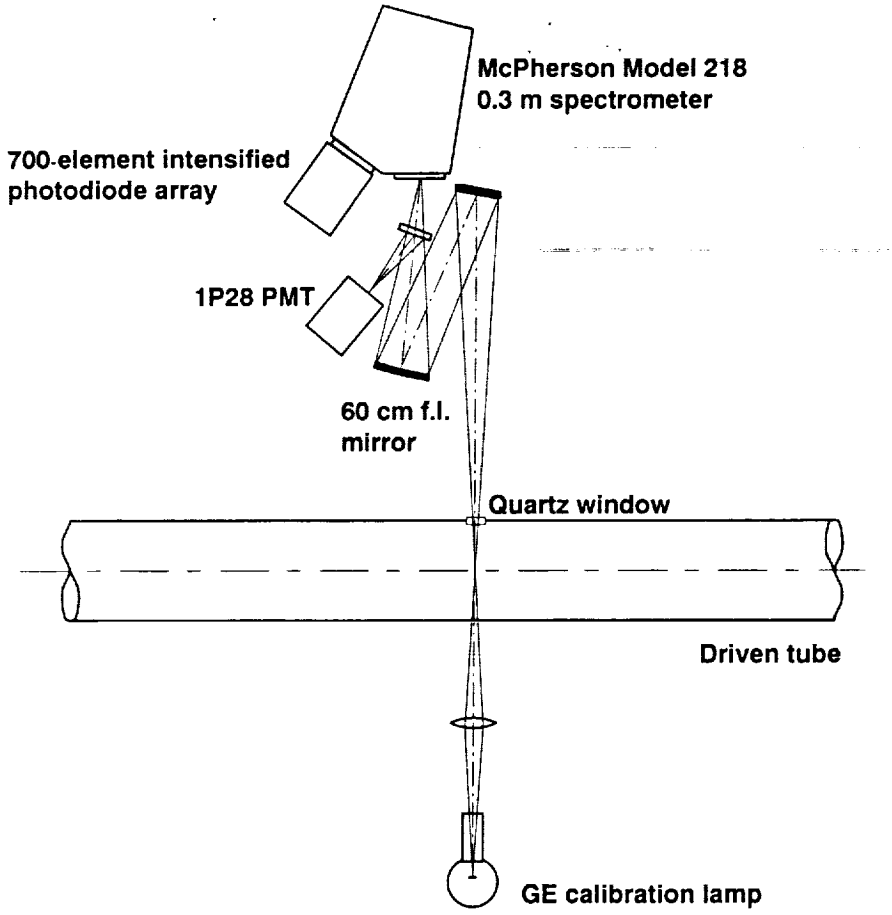

Figure 11. Schematic of shock tube emission spectra collection optics for diode array system.

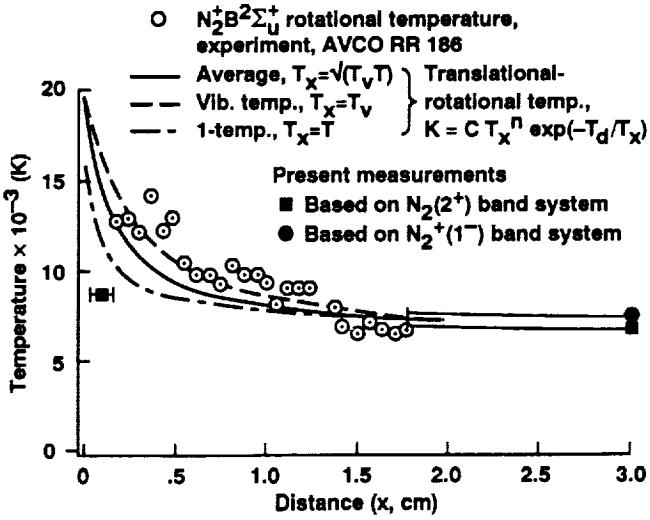

Figure 12. Rotational temperature behind normal shock in nitrogen; U_s = 6.2 k/s, p_1 = 1.0 torr.

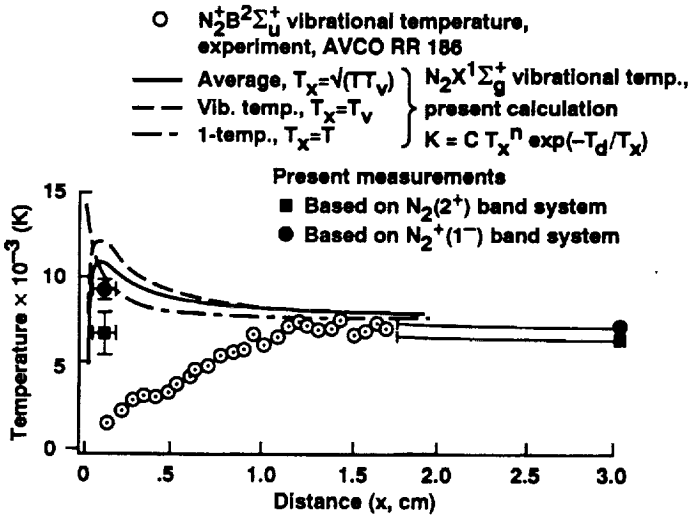

Figure 13. Vibrational temperature behind normal shock in nitrogen; U_s = 6.2 k/s, p_1 = 1.0 torr.

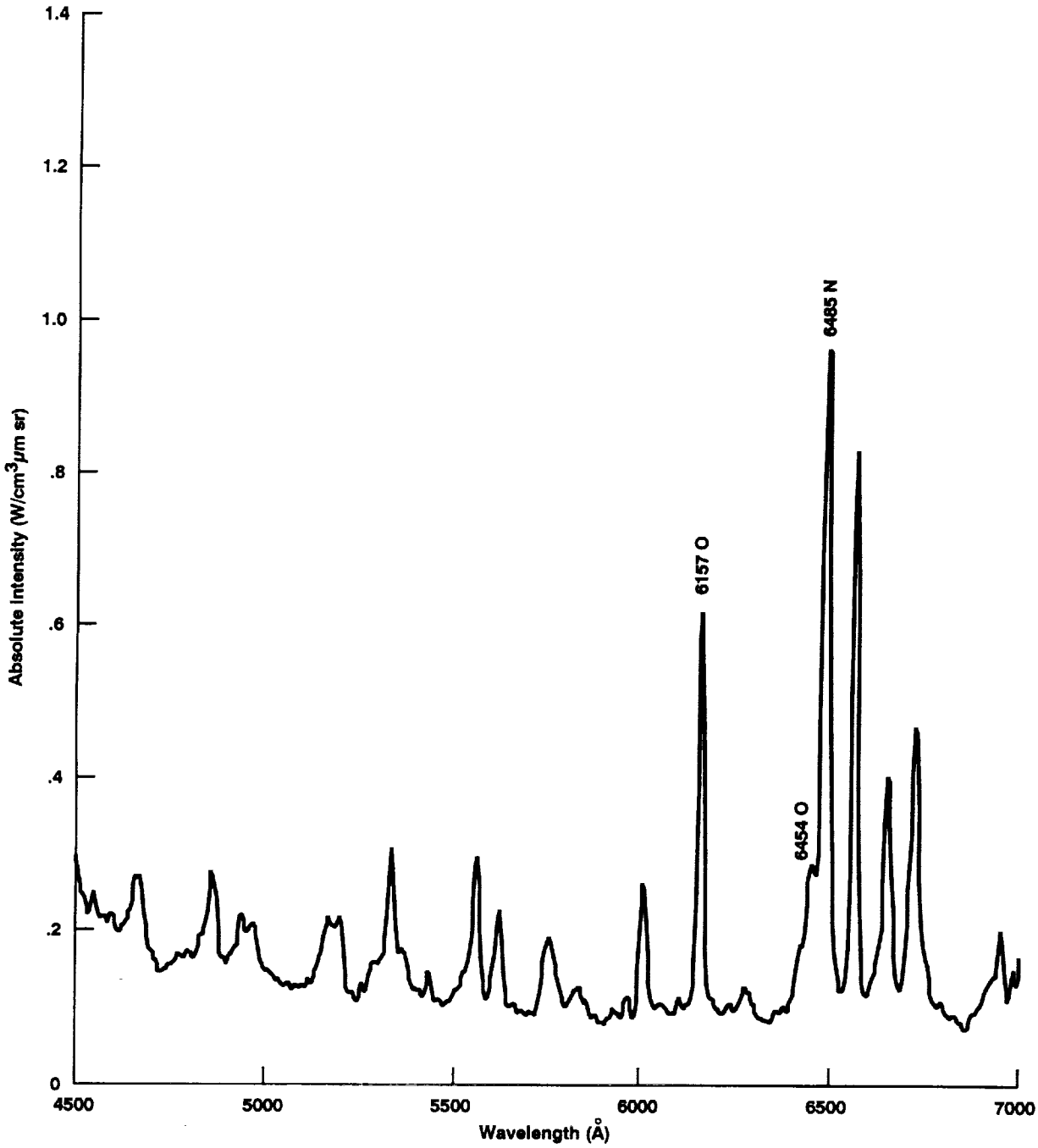

Figure 14. Equilibrium emission spectra behind normal shock in air; U_s = 10.2 k/s, p_1 = 0.1 torr, gate = 1.0 ms, slit = 60 mm.

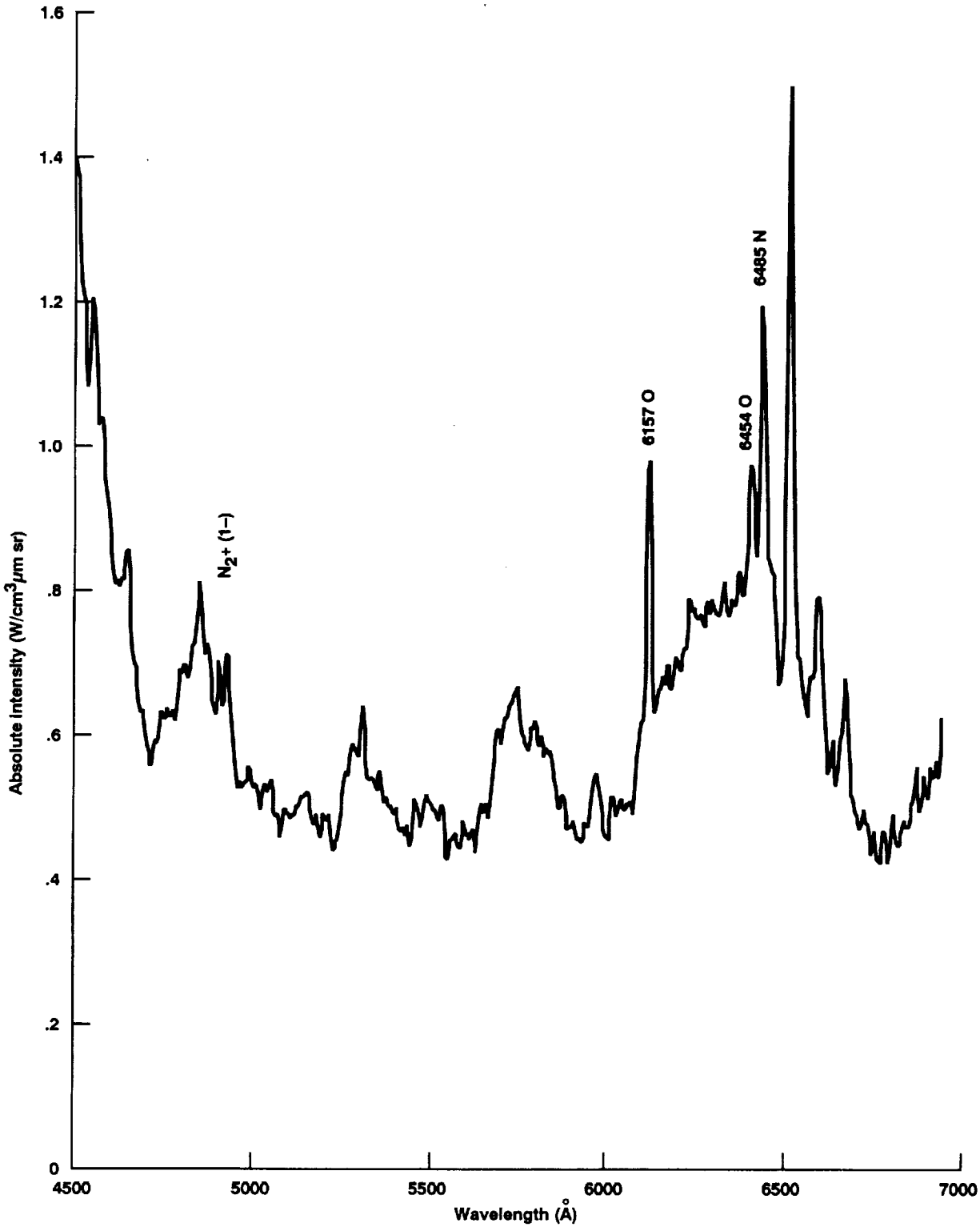

Figure 15. Nonequilibrium emission spectra behind normal shock in air; U_s = 10.2 k/s, p_1 = 0.1 torr, gate = 200 ns, slit = 60 mm.

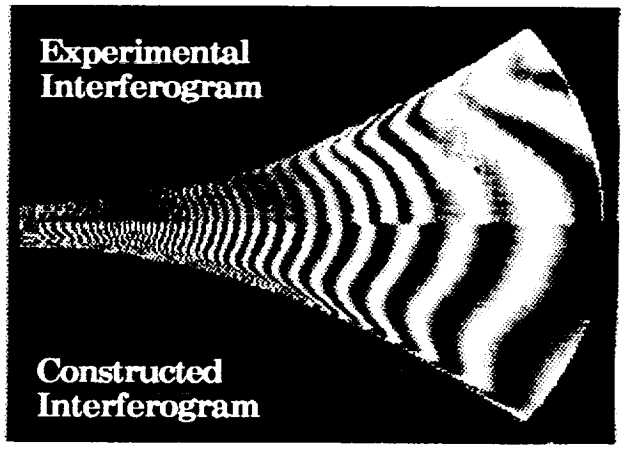

Figure 16. CFD-generated synthetic interferogram compared with experimental observation; P_0 =1530 PSI, T_0 = 7200 K.

REPORT DOCUMENTATION PAGE

Form Approved
OMB No. 0704-0188

1. AGENCY USE ONLY *(Leave blank)*	2. REPORT DATE	3. REPORT TYPE AND DATES COVERED
	October 1992	Technical Memorandum

4. TITLE AND SUBTITLE

Issues and Approach to Develop Validated Analysis Tools for Hypersonic Flows: One Perspective

5. FUNDING NUMBERS

506-40-41

6. AUTHOR(S)

George S. Deiwert

7. PERFORMING ORGANIZATION NAME(S) AND ADDRESS(ES)

Ames Research Center
Moffett Field, CA 94035-1000

8. PERFORMING ORGANIZATION REPORT NUMBER

A-92094

9. SPONSORING/MONITORING AGENCY NAME(S) AND ADDRESS(ES)

National Aeronautics and Space Administration
Washington, DC 20546-0001

10. SPONSORING/MONITORING AGENCY REPORT NUMBER

NASA TM-103937

11. SUPPLEMENTARY NOTES

Point of Contact: George S. Deiwert, Ames Research Center, MS 230-2, Moffett Field, CA 94035-1000; (415) 604-6198

12a. DISTRIBUTION/AVAILABILITY STATEMENT

Unclassified — Unlimited
Subject Category 02

12b. DISTRIBUTION CODE

13. ABSTRACT ***(Maximum 200 words)***

Critical issues concerning the modeling of low-density hypervelocity flows where thermochemical nonequilibrium effects are pronounced are discussed. Emphasis is on the development of validated analysis tools. A description of the activity in the Ames Research Center's Aerothermodynamics Branch is also given. Inherent in the process is a strong synergism between ground test and real-gas computational fluid dynamics (CFD). Approaches to develop and/or enhance phenomenological models and incorporate them into computational flow-field simulation codes are discussed. These models have been partially validated with experimental data for flows where the gas temperature is raised (compressive flows). Expanding flows, where temperatures drop, however, exhibit somewhat different behavior. Experimental data for these expanding flow conditions are sparse; reliance must be made on intuition and guidance from computational chemistry to model transport processes under these conditions. Ground-based experimental studies used to provide necessary data for model development and validation are described. Included are the performance characteristics of high-enthalpy flow facilities, such as shock tubes and ballistic ranges.

14. SUBJECT TERMS	15. NUMBER OF PAGES
Hypersonic flow, Computational fluid dynamics, CFD, CFD validation, Real gas flow	22
	16. PRICE CODE A03

17. SECURITY CLASSIFICATION OF REPORT	18. SECURITY CLASSIFICATION OF THIS PAGE	19. SECURITY CLASSIFICATION OF ABSTRACT	20. LIMITATION OF ABSTRACT
Unclassified	Unclassified		